

Active Nematics

Julia M Yeomans

*The Rudolf Peierls Centre for Theoretical Physics,
Clarendon Laboratory, Parks Road, Oxford, OX1 3PU, UK
Julia.Yeomans@physics.ox.ac.uk*

INTRODUCTION

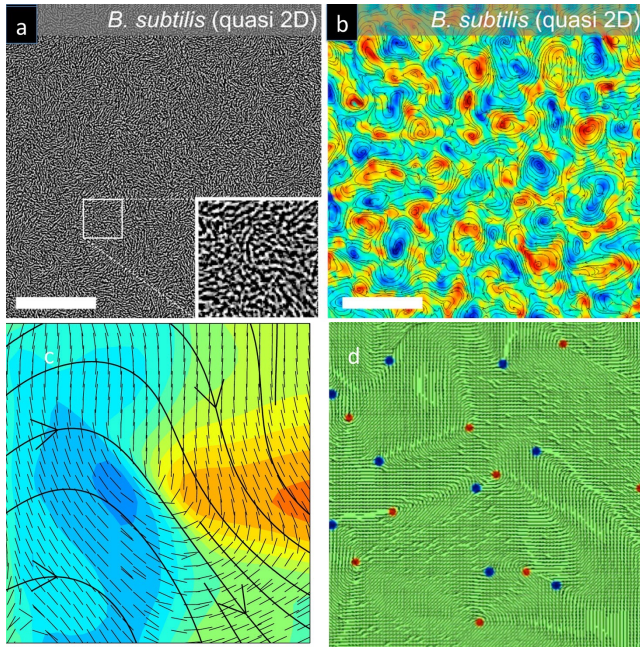


FIG. 1. **Active turbulence:** (a) in a dense suspension of swimming bacteria. (b) The associated vorticity field. Red (blue) regions correspond to high positive (negative) vorticity. Simulations of active turbulence at a smaller length scale. The bend deformation drives a velocity jet (black flow lines, with arrows). (d) Snapshot from simulations showing $+1/2$ (red) and $-1/2$ (blue) topological defects. After [1, 2].

we describe the properties of active turbulence and topological defects. We argue that the short-range nematic ordering required for active turbulence can be initiated by the active flows themselves, and therefore that the turbulence can occur in a system that is isotropic in the passive limit.

The interplay of surfaces, interfaces and activity leads to rich physics and we describe how active nematics behave in confined geometries, and as friction screens the flow. The majority of the experimental and theoretical work so far has been in two dimensions. However active turbulence has now been identified and studied in three dimensions, where the $\pm 1/2$ defects are replaced by active disclination lines and loops. We summarise how active dislocations and active anchoring can drive shape changes in active droplets and shells.

Active nematics are reviewed in [3–5].

Self-propelled active particles create dipolar flow fields which have nematic symmetry. A result of this is that the continuum equations of motion needed to describe dense active particles with hydrodynamic interactions closely resemble those for passive liquid crystals, but with an additional active stress. The new term has far reaching consequences. Long-range nematic order is destroyed by the active flow and replaced by active turbulence, a chaotic flow state with strong vorticity (Fig. 1). In a two-dimensional, passive, nematic defects usually approach each other, driven by elastic interactions, and then annihilate in pairs of topological charge $+1/2$ and $-1/2$. In an active nematic the flow of energy means that defects can also be created in pairs. Moreover a consequence of the active stress is that the defects are self motile. Hence active turbulence is characterised by a dynamic gas of defects that are continually being created, moving around and annihilating.

Active turbulence relies on particles that are elongated in shape or deformable to give local nematic ordering. Examples of active nematics include dense suspensions of microswimmers, bacterial colonies, biological filaments driven by motor proteins, and confluent cell layers and tissues.

This chapter introduces the continuum equations of motion that can be used to describe these materials, and motivates the form for the active stress. We then outline how active flows lead to instabilities, and thence to active turbulence, and

ACTIVE NEMATOHYDRODYNAMICS

Equations of motion

The continuum dynamics of an active nematic is described by coupled equations for the velocity, \mathbf{u} , and the order parameter, $\mathbf{Q} = \frac{d}{d-1}S(\mathbf{n}\mathbf{n} - \mathbf{I}/d)$, where \mathbf{n} is the director, S is the magnitude of the nematic order and d is the dimensionality of space. \mathbf{Q} evolves according to [6]

$$\partial_t \mathbf{Q} + \mathbf{u} \cdot \nabla \mathbf{Q} - \mathbf{S} = \Gamma \mathbf{H}. \quad (1)$$

In addition to advection by the flow, accounted for by the first two terms in this equation, elongated particles respond to flow gradients in a way captured by the co-rotational term,

$$\mathbf{S} = (\lambda \mathbf{E} + \mathbf{\Omega}) \cdot \left(\mathbf{Q} + \frac{\mathbf{I}}{3} \right) + \left(\mathbf{Q} + \frac{\mathbf{I}}{3} \right) \cdot (\lambda \mathbf{E} - \mathbf{\Omega}) - 2\lambda \left(\mathbf{Q} + \frac{\mathbf{I}}{3} \right) (\mathbf{Q} : \nabla \mathbf{u}), \quad (2)$$

where $\mathbf{\Omega}$ and \mathbf{E} are the vorticity and the rate of strain tensors respectively. The relative dominance of the rate of strain and the vorticity in affecting the alignment of nematogens with the flow is characterised by the tumbling parameter λ .

The $\Gamma \mathbf{H}$ term describes relaxational dynamics of the nematic tensor to the minimum of a free energy through a molecular field defined by

$$\mathbf{H} = -\frac{\delta \mathcal{F}}{\delta \mathbf{Q}} + \frac{\mathbf{I}}{3} \text{Tr} \left(\frac{\delta \mathcal{F}}{\delta \mathbf{Q}} \right), \quad (3)$$

with Γ the rotational diffusivity. The free energy is typically taken to have the usual Landau-de Gennes form [7]

$$\mathcal{F}_b = \frac{A}{2} \mathbf{Q}^2 + \frac{B}{3} \mathbf{Q}^3 + \frac{C}{4} \mathbf{Q}^4 + \frac{K}{2} (\nabla \mathbf{Q})^2, \quad (4)$$

where the coefficients of the bulk terms A , B , C are material parameters, and the final term describes the elastic free energy cost of spatial inhomogeneities in the order parameter field, assuming a single elastic constant K .

The velocity field, assuming a constant density ρ , obeys the incompressible Navier-Stokes equations:

$$\nabla \cdot \mathbf{u} = 0, \quad (5)$$

$$\rho (\partial_t \mathbf{u} + \mathbf{u} \cdot \nabla \mathbf{u}) = \nabla \cdot \mathbf{\Pi}. \quad (6)$$

Many active particles are sufficiently small that the low Reynolds number limit is appropriate and the left-hand side of Eq. (6) can be neglected. $\mathbf{\Pi}$ is the stress tensor. It includes the pressure, P , the usual viscous stress,

$$\mathbf{\Pi}^{\text{viscous}} = 2\eta \mathbf{E}, \quad (7)$$

where η is the viscosity, and the elastic stress which describes the backflow induced by any motion of the nematic particles,

$$\mathbf{\Pi}^{\text{elastic}} = 2\lambda (\mathbf{Q} + \mathbf{I}/3) (\mathbf{Q} : \mathbf{H}) - \lambda \mathbf{H} \cdot (\mathbf{Q} + \frac{\mathbf{I}}{3}) - \lambda (\mathbf{Q} + \frac{\mathbf{I}}{3}) \cdot \mathbf{H} - \nabla \mathbf{Q} \frac{\delta \mathcal{F}}{\delta \nabla \mathbf{Q}} + \mathbf{Q} \cdot \mathbf{H} - \mathbf{H} \cdot \mathbf{Q}. \quad (8)$$

The active stress

Equations (1)–(8) describe a passive nematic. The simplest additional term that can account for the stresses induced by active particles is

$$\mathbf{\Pi}^{\text{active}} = -\zeta \mathbf{Q} \quad (9)$$

where ζ is the activity coefficient. An argument to motivate Eq. (9) was given by Simha and Ramaswamy [8]. By Newton's third law the forces on a self-propelled particle must be equal and opposite. Averaging over the details of the swimming stroke, a simple model of a self-propelled particle i which gives the correct far flow field is a rod centred at \mathbf{x}_i along $\hat{\mathbf{n}}_i$ with equal and opposite forces $\pm f\hat{\mathbf{n}}_i$ acting at its ends, at $\mathbf{x}_i + a\hat{\mathbf{n}}_i$ and $\mathbf{x}_i - a'\hat{\mathbf{n}}_i$. Hence the force per unit volume due to the swimmers is

$$\begin{aligned} f_\alpha^{\text{active}}(\mathbf{x}) &= \sum_i f\hat{n}_{i,\alpha} \{ \delta[\mathbf{x} - \mathbf{x}_i - a\hat{\mathbf{n}}_i] - \delta[\mathbf{x} - \mathbf{x}_i + a'\hat{\mathbf{n}}_i] \} \\ &\approx -\frac{(a+a')}{2} \sum_i f\nabla_\beta \hat{n}_{i,\beta} \hat{n}_{i,\alpha} \delta[\mathbf{x} - \mathbf{x}_i] \end{aligned} \quad (10)$$

where the second line of this equation follows from expanding the δ -functions and we have used Greek indices with the usual Einstein summation convention to represent Cartesian directions. Recalling the relation between force and stress

$$\nabla \cdot \mathbf{\Pi}^{\text{active}} \equiv \mathbf{f}^{\text{active}} \quad (11)$$

the leading order contribution to the active stress is

$$\Pi_{\alpha\beta}^{\text{active}} = -(a+a') \sum_i f\hat{n}_{i,\beta} \hat{n}_{i,\alpha} \delta[\mathbf{x} - \mathbf{x}_i]. \quad (12)$$

Coarse-graining, we may replace $\hat{\mathbf{n}}_i$ by the director \mathbf{n} and the sum over i by the concentration of active particles $c(\mathbf{x})$

$$\Pi_{\alpha\beta}^{\text{active}} = -(a+a')c(\mathbf{x})n_\alpha n_\beta. \quad (13)$$

From the definition of the \mathbf{Q} -tensor, and noting that constant terms in the stress do not affect the dynamics, Eq. (9) follows immediately. The unknown microscopic parameters, which depend on the details of the active forces, and the concentration of active particles determine the activity ζ . $\zeta > 0$ corresponds to extensile particles that pump fluid outwards away from their ends and $\zeta < 0$ to contractile particles that draw fluid inwards towards their ends. Note that the form of the active stress remains the same for both polar ($a \neq a'$) and apolar ($a = a'$) active particles.

Exercise 1: Deriving the active stress.

Starting from Eq. (10) follow through the steps that lead to the expression for the active stress, filling in details.

Active instabilities

$\mathbf{\Pi}^{\text{active}}$ appears under a derivative in the equations of motion. Thus any gradient in the direction or magnitude of the nematic field induces stresses and hence flows. Linear stability analysis shows that a far-reaching consequence is that the homogeneous nematic phase is unstable to active stresses [8, 9].

We assume that the director is oriented along the x -direction and calculate how small perturbations to the nematic order evolve with time. The elements of the perturbed nematic tensor are $Q_{xx} = Q_{xx}^0 + \delta Q_{xx}$ and $Q_{xy} = Q_{xy}^0 + \delta Q_{xy}$ where $(Q_{xx}^0, Q_{xy}^0) = (S_0/2, 0)$. Using Eqs. (1) and (6), representing the Fourier transform of any fluctuating field δf as $\delta f(\mathbf{r}, t) = \int d\mathbf{q} \tilde{f}(\mathbf{q}, t) e^{i\mathbf{q}\cdot\mathbf{r}}$, and setting $\lambda = 0$ for simplicity, the evolution of the perturbations in the low-Reynolds number limit are

$$\partial_t \tilde{Q}_{xx} = -\tilde{Q}_{xx}(Kq^2 + 2S_0^2 A)\Gamma, \quad (14)$$

$$\partial_t \tilde{Q}_{xy} = -\tilde{Q}_{xy} \{ K\Gamma q^2 - (2\eta)^{-1} S_0 \zeta \cos 2\theta \} - (2\eta)^{-1} \tilde{Q}_{xx} \sin 2\theta S_0 \zeta \quad (15)$$

where θ is the angle between \mathbf{q} and the nematic director. Eq. (14) shows that the longitudinal perturbations relax to zero and Eq. (15) gives the growth rate of transverse perturbations \tilde{Q}_{xy} as

$$\omega = -\{K\Gamma q^2 - (2\eta)^{-1}S_0\zeta \cos 2\theta\}. \quad (16)$$

For $\omega < 0$, perturbations die out over time whereas for $\omega > 0$ perturbations grow and long-range nematic order is unstable. Fig. 2 indicates pictorially how the instability in an extensile active nematic leads to destabilising flows.

Exercise 2: Active instabilities.

a. What type of nematic distortion drives the instability in (i) extensile ($\zeta > 0$), (ii) contractile ($\zeta < 0$) active nematics?

b. Draw a diagram illustrating the formation of the instability for a contractile active nematic. Hint: see Fig. 2 for the extensile case.

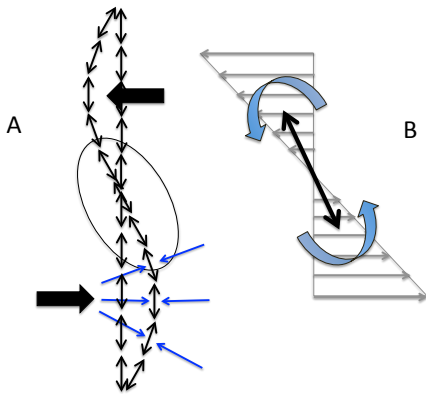


FIG. 2. **Instability in an extensile active nematic:** A: each nematogen in the distorted configuration produces flow shown in blue. The flow is unbalanced giving a resultant vortical flow shown as large black arrows. B: The shear acts to increase the deformation destabilising the ordered nematic state (courtesy of S. P. Thampi).

continuously being created and destroyed. The flow field, driven by stresses due to defects and other director gradients is highly chaotic. Vortices form over a range of length scales, with areas that are exponentially distributed [13]. The active length scale, which governs the decay of the vorticity correlations is $\sqrt{(K/\zeta)}$. Snapshots of active turbulence are shown in Fig. 1.

Active turbulence is markedly different from inertial turbulence, as one might expect given the very different Reynolds number. In active turbulence (Reynolds number very small) the energy input is at the scale of the individual particles, and the energy is dissipated on the scale of the vortices. In inertial turbulence (Reynolds number very large) energy is input at large scales and cascades to smaller scales. A detailed statistical analysis of active turbulence indeed shows a clear distinction from inertial turbulence in terms of intermittency, energy spectrum, and flow structure [14].

ACTIVE TURBULENCE

Long-range nematic order is destroyed by active flows, but how do the instabilities grow beyond the linear regime? Numerical solutions of the active nematohydrodynamic equations have helped to answer this question, showing that the system settles into a state, termed active or mesoscale turbulence, which is characterised by strong fluid jets and high vorticity in the flow field, and short-range nematic order and motile topological defects in the director field [10, 11].

Fig. 3 illustrates the onset of active turbulence. The distortions created by the hydrodynamic instabilities tend to localise to form *walls*, lines of high distortion separated by nematic regions. Because of their high elastic energy the walls are preferential sites for the formation of $\pm 1/2$ topological defects. Rather than immediately annihilating, local stresses cause the $+1/2$ defect to move away from the $-1/2$ defect. The defects initially tend to move along walls but their dynamics, together with that of the walls, rapidly becomes chaotic. If oppositely charged defects encounter each other they annihilate [12].

Hence a dynamical steady state results, with motile defects

continuously being created and destroyed. The flow field, driven by stresses due to defects and other director gradients is highly chaotic. Vortices form over a range of length scales, with areas that are exponentially distributed [13]. The active length scale, which governs the decay of the vorticity correlations is $\sqrt{(K/\zeta)}$. Snapshots of active turbulence are shown in Fig. 1.

Active turbulence is markedly different from inertial turbulence, as one might expect given the very different Reynolds number. In active turbulence (Reynolds number very small) the energy input is at the scale of the individual particles, and the energy is dissipated on the scale of the vortices. In inertial turbulence (Reynolds number very large) energy is input at large scales and cascades to smaller scales. A detailed statistical analysis of active turbulence indeed shows a clear distinction from inertial turbulence in terms of intermittency, energy spectrum, and flow structure [14].

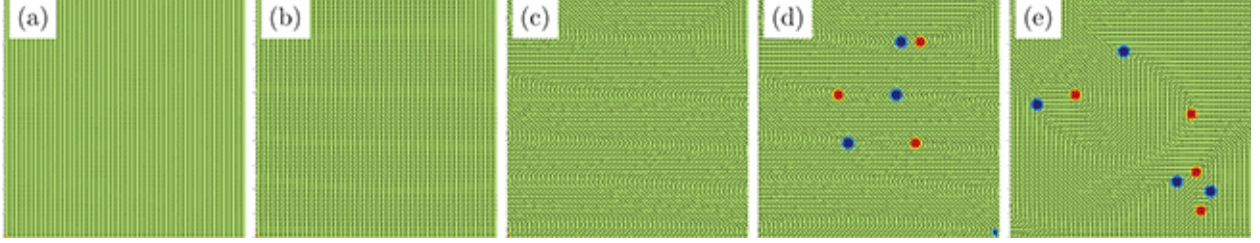


FIG. 3. **Onset of active turbulence:** Snapshots at successive times of the director field (dashed lines) and $+1/2$ and $-1/2$ defects (red and blue, respectively) during the development of active turbulence from an ordered nematic state (a) for an extensile system. Walls are formed (b) and sharpen (c). Defect pairs appear at walls (d). Initially they move along the walls (and restore nematic order) but their motion quickly becomes chaotic (e). After [12]. An experiment showing this instability is described in [16].

As an alternative to the continuum equations, an approach based on kinetic theory, has been used to model the nematohydrodynamics of active, rod-like particles [15]. Each particle is represented as a slender rod with a surface velocity that results in extensile or contractile dipolar flows, and the distribution function for the number density of the particles is described by the Smoluchowski equation. The particle concentration and nematic tensor are then constructed from the first and second moments of the distribution function, and the centre of mass position and orientation of the rods are found from slender body theory for zero-Reynolds number flows. Such a kinetic theory approach is able to reproduce the generation of active turbulence and the dynamics of active defects.

Motile topological defects

Topological defects are regions of high director distortion and hence they act as sources of stress and flow. A calculation by Giomi *et al.* [17] has shown that it is possible to obtain the velocity field of defects analytically under certain approximations. The director field of a point defect is $\mathbf{n} = (\cos m\phi, \sin m\phi)$ where ϕ is the polar angle and m is the topological charge of the defect. The body force due to activity follows immediately as

$$\mathbf{f}^{\text{active}} = \nabla \cdot \mathbf{\Pi}^{\text{active}} = \frac{\zeta}{2r} \hat{\mathbf{x}}, \quad m = +1/2, \quad (17)$$

$$= \frac{\zeta}{2r} (-\cos 2\phi \hat{\mathbf{x}} + -\sin 2\phi \hat{\mathbf{y}}), \quad m = -1/2. \quad (18)$$

Within the Stokes' approximation the velocity induced by this force field is

$$v_i(\mathbf{r}) = \int dA' G_{ij}(\mathbf{r} - \mathbf{r}') f_j(\mathbf{r}') \quad (19)$$

where G_{ij} is the two-dimensional Oseen tensor

$$G_{ij}(\mathbf{r}) = \frac{1}{2\pi\eta} \left\{ \left(\log \frac{R}{r} - 1 \right) \delta_{ij} + \frac{r_i r_j}{r^2} \right\}. \quad (20)$$

Substituting the active force distribution (18) into equation (19) and using (20) gives (see the appendix of [17] for details)

$$v_+^a(r, \phi) = \frac{\zeta}{12\eta} \{ (3(R-r) + r \cos 2\phi) \hat{\mathbf{x}} + r \sin 2\phi \hat{\mathbf{y}} \} \quad (21)$$

for the velocity field produced by a $+1/2$ defect and

$$v_-^a(r, \phi) = \frac{\zeta r}{12\eta R} \{((3r/4 - R) \cos 2\phi - R \cos 4\phi/5)\hat{x} + ((3r/4 - R) \sin 2\phi + R \sin 4\phi/5)\hat{y}\} \quad (22)$$

for a $-1/2$ defect.

To obtain these formulas it is necessary to make assumptions about the extent of the domain and the behaviour of the director and velocity fields on its boundaries. The choice used here is that outside a radius R the director field is uniform and that there are no slip conditions on the velocity field at R . In active turbulence the cut off is most likely to be provided by other defects.

Under the assumption that the convective dynamics of the flow dominates director relaxation the defect can be considered as a particle moving at the velocity of its core. Putting $r = 0$ in Eqns. (21) and (22) gives an estimate for the velocity of $+1/2$ defects, $(\zeta R/4\eta) \hat{x}$, and confirms that $-1/2$ defects are not self-propelled.

Exercise 3: Active topological defects.

- a. Use the expressions (21) and (22) to plot the flow field around a $+1/2$ and a $-1/2$ active defect.
- b. From the literature, find (at least) five different experimental systems where active topological defects have been identified.

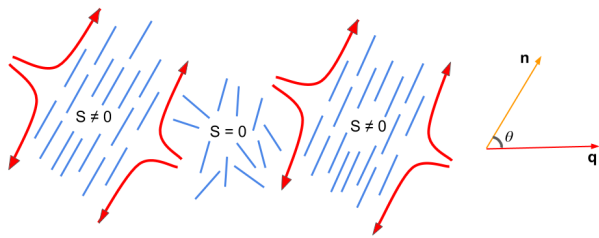


FIG. 4. **Activity-induced nematic ordering** in an isotropic system of active particles. Blue solid lines indicate nematic directors and red arrows denote the activity-induced flows. The disordered region at the centre is aligned by the shear flow set up by the neighbouring ordered regions.

Activity-driven active turbulence

A second, competing, instability is also relevant to the behaviour of active nematics [18–20]. If the thermodynamic parameters are chosen so that the passive liquid crystal is in the isotropic phase, short-range nematic order and active turbulence can still be observed. This occurs because local fluctuations in the magnitude of the nematic order set up shear flows which can, in turn, enhance the ordering. A stability analysis shows that the critical wave number below which the system is unstable is

$$q_c = \sqrt{\frac{\lambda\zeta}{2K(2\eta\Gamma + \lambda^2)}}. \quad (23)$$

Hence the instability only occurs if $\lambda\zeta > 0$, for extensile, rod-like particles or contractile, disc-shaped particles that align in a shear flow.

A diagram showing the physical mechanism involved in the creation of nematic order is shown in Fig. 4. Each active particle creates a dipolar flow field. The dipole lies along the long axis of the particle, and extensile particles pull fluid in from their sides and push it out from their ends. In a perfectly isotropic arrangement of active particles the dipolar flows generated by each particle cancel each other on sufficiently large length scales so there is no net flow. However, if a fluctuation generates a local nematic alignment of active particles, then this results in the generation of locally shearing flow fields. In such shear flows particles align further in a manner that enhances the shear. This again results in the strengthening of the nematic

order creating a bootstrap effect: stronger alignment leads to stronger flows that in turn generate stronger alignment ... but this process will be balanced by the instability that we described earlier, the destruction of long-range nematic ordering by flow, which will be occurring simultaneously.

Experimental systems

An early identification of active turbulence was in suspensions of *Bacillus subtilis* swimming near the contact line of a sessile drop [21]. Since then it has become apparent that this is a generic behaviour of many dense suspensions of microswimmers. Another nematic model system is *living liquid crystals*. These are bacteria dispersed in aqueous-based liquid crystals, a set-up which allows the swimming characteristics of the bacteria and the orientational order of the medium to be controlled independently [22]. The bacteria align along the director of the liquid crystal and motility is tuned by the amount of dissolved oxygen. After an oxygen supply is initiated, bacteria start swimming and trigger a stripe-like instability that, at sufficiently high activity, gives rise to the nucleation of half-integer defects proliferating into active turbulence. Flows resembling active turbulence are also seen in assemblies of bacterial cells crawling on a surface although here friction is expected to screen the hydrodynamic interactions. An example is *Pseudomonas aeruginosa* which uses pili, hair like appendages, to pull itself along [23].

A particularly important experimental system that has been key in investigating the properties of active turbulence is a dense mixture of microtubules, biopolymers about $1.5 \mu\text{m}$ in length, and double-headed versions of the motor protein kinesin, driven by ATP [24]. The addition of the depleting agent PEG concentrates the microtubules into bundles. The microtubules are polar and the kinesin bridges between pairs of microtubules and walks towards the plus end. If the microtubules are parallel there is no net displacement, but if they are antiparallel the microtubules move relative to each other and this results in polarity-sorted bundles of the biopolymers. The bundles are not stable but buckle and fracture leading to the dynamical steady-state of active turbulence. In many experiments, the active microtubule and motor protein mixture assembles at an oil-water interface giving a two dimensional active layer where properties such as the velocity-velocity correlation function and the trajectories of active defects can be measured. More recently three-dimensional assays have been developed by enhancing the nematic ordering by adding a passive colloidal liquid crystal based on filamentous viruses [25].

Perhaps more surprisingly, active turbulence and motile topological defects have been observed in confluent cell layers. Epithelial cells are tightly connected by means of cell-cell junctions and active inter-cellular forces constantly drive deformations of the shapes of the cells. By mapping out the (coarse-grained) direction of the long axis of the deformed cells, Saw et al. [26] identified nematic order and motile topological defects within a two-dimensional confluent layer of epithelial MDCK cells. The flow fields and stresses around the defects were in agreement with active nematic theories, and experiments showed that there is a correlation between the level of activity (controlled in the experiments by adding blebbistatin) and the number of defects in the cell layer. Kawaguchi et al. [27] worked with neural progenitor cells, showing that, at high densities and under confinement, they are capable of aligning over long length scales, forming migratory streams. The cells tended to deplete the neighbourhood of $-1/2$ defects and instead to accumulate at $+1/2$ defects, forming mounds. Following these papers, active turbulence and topological defects are now being identified in an increasing number of cell monolayers.

CONFINEMENT

When active nematics are confined the hydrodynamics is screened and active turbulence can be replaced by more regular flows. These depend sensitively not only on the fluid parameters and the confinement dimensions but also on the boundary conditions and the strength of intrinsic fluctuations. Simulations of active flow in a one-dimensional channel show that, as the *activity number*, $A = \sqrt{(\zeta h^2)/K}$, where h is the channel height, is increased the change in flow configurations is from no flow \rightarrow laminar flow (shear or unidirectional) \rightarrow a one-dimensional line of flow vortices \rightarrow active turbulence (Fig. 5) [28]. The system starts

to flow when the active stresses can overcome the pinning effect of the boundaries, velocity vortices can form once the channel becomes wide enough to accommodate them, and then a further increase in channel width allows relative motion of the vortices, corresponding to active turbulence.

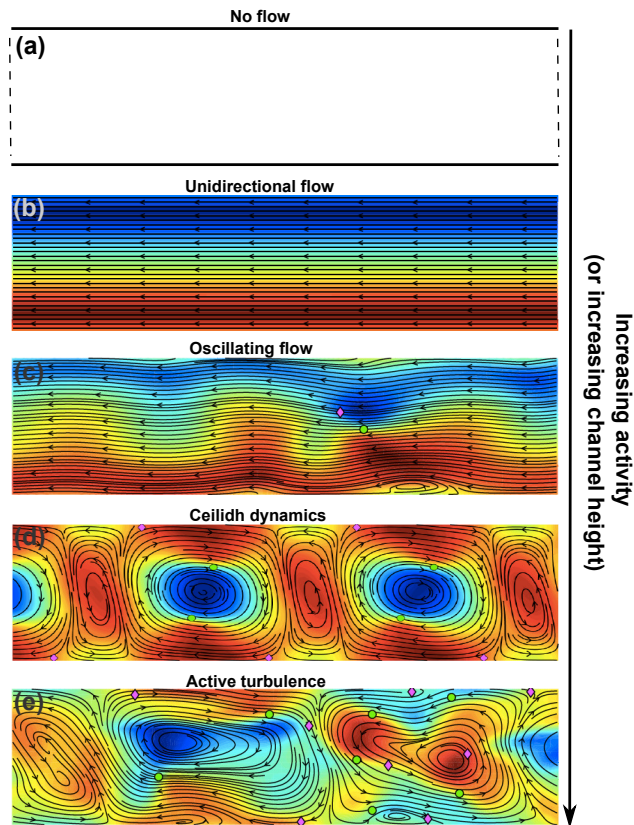


FIG. 5. **Channel flow**; Flow states of an active nematic confined in a channel. The black lines are the streamlines of the velocity field and the colourmap represents the vorticity field. Circles (green) and diamonds (magenta) mark $+1/2$ and $-1/2$ topological defects. After [29].

a stripe on a micro-patterned glass substrate [32]. Experiments on microtubule-motor protein bundles correspond to higher activity numbers. By changing the channel width Hardouin et al. [33] were able to demonstrate the transitions from laminar (shear) flow, to a flow-vortex state with dancing defects, and then to active turbulence. The experiments identified a state where well-defined shear flow alternates in a regular way with bursts of instability characterised by $+1/2$ topological defects moving across the channel. This occurs because the shear aligns the microtubules parallel to the walls so that they then undergo the usual active instability, bending to create defect pairs

Friction

Friction, with external fluids or boundaries, screens hydrodynamic flows and leads to a crossover from a *wet* to a *dry* system. It has a complex effect on the properties of active nematics and is likely to be important in many experiments.

The motile, active defects add complexity to this sequence. Channel walls are preferential sites for defect formation. The stationary $-1/2$ defects remain close to the walls due to elastic interactions, whereas the self-propelled $+1/2$ defects move toward the centre of the channel. $+1/2$ defects can traverse the channel to be annihilated by the $-1/2$ defects at the opposite wall. In the vortex regime, however, they can alternatively be captured by the flow vortices and perform a *ceilidh dance*, with right- and left-moving defects moving past each other on sinusoidal trajectories in a way reminiscent of the great chain figure in country dancing. Similar interplays between active flow and the dynamics of motile topological defects govern the behaviour of active materials confined to circles [30].

The transition from the flow vortex lattice to active turbulence in a channel has interesting properties. Turbulent patches continually appear, combine and die out, giving a kymograph (space-time diagram) reminiscent of directed percolation [31]. Measuring the behaviour of the transition where the turbulent cluster first spans the system indicates that it is indeed in the directed percolation universality class. The same behaviour is associated with the transition to inertial turbulence in channel flow.

The confinement flows have been observed in experiments, although different systems are needed to probe different activity numbers. Confluent cell layers correspond to low activities and the transition from a quiescent state to flow has been observed in layers of spindle-shaped cells confined to

For active nematics with strong thermodynamic ordering, friction introduces a memory into the system so that the motion of topological defects leaves trails, arch-like distortions in the director field, that persist for a time that increases with increasing friction. Defects in both extensile and contractile systems move in the same direction with respect to the polar axis of arches. They interact with the trails left by other defects, which leads to a polar order of the $+1/2$ defects. At very high friction there is insufficient energy to create new topological defects, but if there are defects already in the system they create arches in the director field before eventually annihilating. The arches align parallel to each other and readjust to equal widths to form regular arch patterns that coexist with the nematic phase [34]. For active nematics with activity-induced ordering, however, it is much easier to create topological defects. The number of defects proliferate with increasing friction and elastic and hydrodynamic interactions lead to nematic defect ordering on length scales many times larger than the active length scale [35].

If the friction is anisotropic so that the nematogens move more easily along than perpendicular to their length, yet other flow states and defect configurations are possible. If the active particles are flow-aligning the chaotic flows can be streamlined into flow lanes with alternating directions, and widths large compared to the active length scale. This reproduces the laning state that has been observed in experiments by interfacing microtubule-motor protein mixtures with smectic liquid crystals. By contrast, for flow tumbling particles, the synergistic effects of friction anisotropy and flow tumbling can lead to the emergence of bound pairs of active defects that align at an angle to the easy flow direction and move together [36].

THREE DIMENSIONS

Three-dimensional active turbulence is again characterised by spatiotemporally chaotic flows. However, point defects are replaced by disclination lines which constantly undergo transformation events such as breakup, recombination, nucleation and annihilation. In bulk systems disclination lines typically form closed, charge-neutral loops [25]. However, they can also terminate at surfaces and the dynamics of the resultant defects on the surface is coupled to the disclination line dynamics in the bulk by elastic interactions and flows [37].

Disclination lines can continuously transform from a local $-1/2$ configuration in the plane perpendicular to the line into a $+1/2$ configuration through an intermediate twist winding as indicated in Fig. 6. Moving around the core of a disclination in the plane perpendicular to the local disclination line segment, the director field winds around a specific axis, the rotation vector Ω (black arrows) by an angle π . The angle β between Ω and the local line tangent \mathbf{t} (yellow arrow) is called the *twist angle* and can be used to locally characterise the disclination line. For $-1/2$ ($+1/2$) wedge-type defects the twist angle corresponds to $\beta \approx 0(\pi)$, while line segments with local twist-type defects are indicated by $\beta \approx \pi/2$.

As a consequence of the activity, disclination lines act as self-propelled entities moving through the fluid. Based on a simplified model neglecting elastic interactions, each disclination line segment can be associated with a local self-propulsion velocity which has a component perpendicular to the local tangent of the line

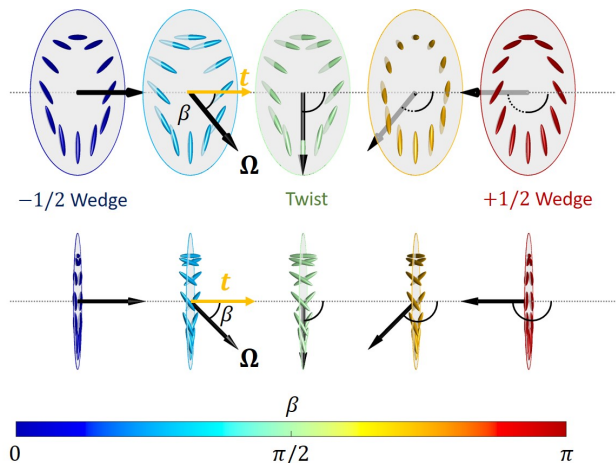


FIG. 6. **Dislocation lines:** A local $-1/2$ wedge can continuously transform into a $+1/2$ wedge via an intermediate twist disclination. The director field winds about the rotation vector Ω (black arrows) by an angle π . The angle between the rotation vector Ω and the local disclination line tangent \mathbf{t} (yellow arrow), called the *twist angle* β , varies continuously along a disclination line. Twist disclinations correspond to $\beta \approx \pi/2$ and $+1/2$ and $-1/2$ wedge disclinations to $\beta \approx \pi$ and 0 , respectively. Adapted from [25].

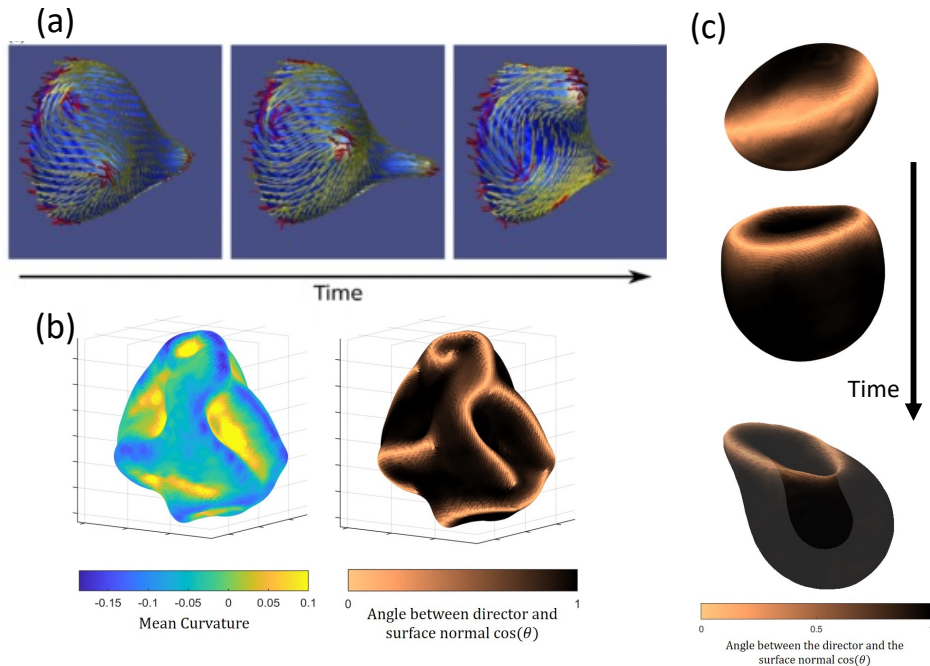


FIG. 7. **Deformable active droplets:** (a) Active shell showing protrusion formation at a $+1/2$ topological defect. After [38]. (b) Wrinkle formation in a contractile active droplet. (c) Invagination of a smaller contractile active droplet. After [39]. These results were obtained by solving the active nematohydrodynamic equations using a hybrid lattice Boltzmann algorithm.

which depends on the twist angle β as [40]

$$v_{\perp}^{SP} \propto (1 - \cos \beta)^2. \quad (24)$$

Thus line segments with $\beta = 0$ are passive while $\beta = \pi$ line segments are most active in pushing around the surrounding fluid and distorting the dislocation loops.

A combination of activity, defect and disclination dynamics, and active anchoring can lead to an enormous range of behaviours in deformable active drops and shells. Fig. 7(a) shows simulations of a deformable active shell (with the director field strongly anchored to lie within the shell). The extending protrusion is caused by flows normal to the surface initiated near a $+1/2$ topological defect [38]. Analogous behaviour has been implicated in driving tentacle formation in the marine polyp *Hydra* [41].

Fig. 7(b) shows simulations of a contractile deformable droplet. The wrinkles that form are related to points where dislocation lines reach the surface. Fig. 7(c) shows the time evolution of a contractile droplet, but now a much smaller one. In contractile systems active flows favour normal surface alignment and hence there is at least one $+1$ disclination-loop in the bulk due to topological constraints. These loops are associated with a large elastic energy cost. Therefore a ring with in-plane surface alignment is formed encircling the droplet to maximize the area of perpendicular surface alignment favoured by active anchoring while avoiding the formation of the $+1$ defect-loop in the bulk. The contractile activity of this director configuration produces flows that cause the droplet to invaginate, forming a cup shape [39]. A similar transition occurs in gastrulation, the stage of morphogenesis where a single cell sheet reorganises into a multilayer structure which then differentiates into the cell types that will initiate the formation of different organs.

WHAT NEXT?

Active nematics have potential as devices, translating chemical energy to mechanical work. However, to achieve this potential it is necessary to design synthetic active systems that can be produced in bulk and are cheap and easy to handle.

They comprise a large number of particles that behave collectively but remain out of thermodynamic equilibrium. There is a lot of research still to be done to extend the theories of non-equilibrium statistical mechanics that are currently being developed for simpler active systems to active nematics. For example, although we understand a lot about active turbulence from simulations, predictive theories are still at an early stage.

Increasingly the ideas underlying active nematic dynamics are being applied to biological systems. Active turbulence and motile defects have now been observed in many confluent cell layers. It is interesting to ask which additional features are important in biological active flows, and to start to apply the ideas arising from active nematic physics to three-dimensional mechanobiology.

-
- [1] H. H. Wensink, J. Dunkel, S. Heidenreich, K. Drescher, R. E. Goldstein, H. Löwen, and J. M. Yeomans, PNAS **109**, 14308 (2012).
 - [2] S. P. Thampi, A. Doostmohammadi, T. N. Shendruk, R. Golestanian, and J. M. Yeomans, Sci. Adv. **2**, e1501854 (2016).
 - [3] J. Prost, F. Jülicher, and J. F. Joanny, Nat. Phys. **11**, 111 (2015).
 - [4] D. Needleman and Z. Dogic, Nat. Rev. Mat. **2**, 17048 (2017).
 - [5] A. Doostmohammadi, J. Ignes-Mullol, J. M. Yeomans, and F. Sagues, Nature Comms. **9**, 3246 (2020).
 - [6] A. N. Beris and B. J. Edwards, *Thermodynamics of Flowing Systems: With Internal Microstructure* (Oxford University Press, 1994).
 - [7] P. G. de Gennes and J. Prost, *The Physics of Liquid Crystals* (Oxford University Press, 1995).
 - [8] R. A. Simha and S. Ramaswamy, Phys. Rev. Lett. **89**, 058101 (2002).
 - [9] R. Voituriez, J. F. Joanny, and J. Prost, Europhys. Lett. **70**, 404 (2005).
 - [10] L. Giomi, M. J. Bowick, X. Ma, and M. C. Marchetti, Phys. Rev. Lett. **110**, 228101 (2013).
 - [11] S. P. Thampi, R. Golestanian, and J. M. Yeomans, Phys. Rev. Lett. **111**, 118101 (2013).
 - [12] S. P. Thampi, R. Golestanian, and J. M. Yeomans, Europhys. Lett. **105**, 18001 (2014).
 - [13] L. Giomi, Phys. Rev. X **5**, 031003 (2015).
 - [14] J. Urzay, A. Doostmohammadi, and J. M. Yeomans, J. Fluid Mech. **822**, 762 (2017).
 - [15] T. Gao, M. D. Betterton, A. S. Jhang, and M. J. Shelley, Phys. Rev. Fluids **2**, 093302 (2017).
 - [16] B. Martinez-Prat, J. Ignes-Mullol, J. Casademunt, and F. Sagues, Nature Physics **15**, 362 (2019).
 - [17] L. Giomi, M. Bowick, P. Mishra, R. Sknepnek, and M. Marchetti, Philos. Trans. A: Math. Phys. Eng. Sci. **372**, 0365 (2014).
 - [18] S. P. Thampi, A. Doostmohammadi, R. Golestanian, and J. M. Yeomans, Europhys. Lett. **112**, 28004 (2015).
 - [19] T. Gao and Z. Li, Phys. Rev. Lett. **119**, 108002 (2017).
 - [20] S. Santhosh, M. R. Nejad, A. Doostmohammadi, J. M. Yeomans, and S. P. Thampi, Journal of Statistical Physics **180**, 699 (2020).
 - [21] C. Dombrowski, L. Cisneros, S. Chatkaew, R. E. Goldstein, and J. O. Kessler, Phys. Rev. Lett. **93**, 098103 (2004).
 - [22] S. Zhou, A. Sokolov, O. D. Lavrentovich, and I. S. Aranson, PNAS **111**, 1265 (2014).
 - [23] O. J. Meacock, A. Doostmohammadi, K. R. Foster, J. M. Yeomans, and W. M. Durham, Nature Physics **17**, 205 (2021).
 - [24] T. Sanchez, D. T. Chen, S. J. DeCamp, M. Heymann, and Z. Dogic, Nature **491**, 431 (2012).
 - [25] G. Duclos, R. Adkins, D. Banerjee, M. Peterson, M. Varghese, I. Kolvin, A. Baskaran, R. Pelcovits, T. Powers, A. Baskaran, F. Toschi, M. Hagan, S. Streichan, V. Vitelli, D. Beller, and Z. Dogic, Science **367**, 1120 (2020).
 - [26] T. B. Saw, A. Doostmohammadi, V. Nier, L. Kocgozlu, S. Thampi, Y. Toyama, P. Marcq, C. T. Lim, J. M. Yeomans, and B. Ladoux, Nature **544**, 212 (2017).
 - [27] K. Kawaguchi, R. Kageyama, and M. Sano, Nature **545**, 327 (2017).
 - [28] T. N. Shendruk, A. Doostmohammadi, K. Thijssen, and J. M. Yeomans, Soft Matter **13**, 3853 (2017).
 - [29] A. Doostmohammadi and J. M. Yeomans, Eur. Phys. J. Special Topics **227**, 2401 (2019).

- [30] A. Opathalage, M. M. Norton, M. P. Juniper, B. Langeslay, S. A. Aghvami, S. Fraden, and Z. Dogic, Proc. Natl. Acad. Sci. U.S.A. **116**, 4788 (2019).
- [31] A. Doostmohammadi, T. N. Shendruk, K. Thijssen, and J. M. Yeomans, Nat. Commun. **8**, 15326 (2017).
- [32] G. Duclos, C. Blanch-Mercader, V. Yashunsky, G. Salbreux, J.-F. Joanny, J. Prost, and P. Silberzan, Nat. Phys. **14**, 728 (2018).
- [33] J. Hardouin, R. Hughes, A. Doostmohammadi, J. Laurent, T. Lopez-Leon, J. M. Yeomans, J. Iñes-Mullol, and F. Sagues, Communications Physics **2**, 1 (2019).
- [34] M. R. Nejad, A. Doostmohammadi, and J. M. Yeomans, Soft Matter **17**, 2500 (2021).
- [35] K. Thijssen, M. R. Nejad, and J. M. Yeomans, Phys. Rev. Lett. **125**, 218004 (2020).
- [36] K. Thijssen, L. Metselaar, J. M. Yeomans, and A. Doostmohammadi, Soft Matter **16**, 2065 (2020).
- [37] S. Čopar, J. Aplinc, Ž. Kos, S. Žumer, and M. Ravnik, Physical Review X **9**, 031051 (2019).
- [38] L. Metselaar, J. M. Yeomans, and A. Doostmohammadi, Phys. Rev. Lett. **123**, 208001 (2019).
- [39] L. J. Ruske and J. M. Yeomans, Phys. Rev. X **11**, 021001 (2021).
- [40] J. Binysh, Z. Kos, S. Čopar, M. Ravnik, and G. P. Alexander, Phys. Rev. Lett. **124**, 088001 (2020).
- [41] Y. Maroudas-Sacks, L. Garion, L. Shani-Zerbib, A. Livshits, E. Braun, and K. Keren, Nature Physics **17**, 251 (2021).